Bayesian phylodynamics reveals the transmission dynamics of avian influenza A(H7N9) virus at the human-live bird market interface in China

Journal Article

Author(s):
Guinat, Claire [ID]; Tang, Hao; Yang, Qiqi; Valenzuela Agüí, Cecilia; Vaughan, Timothy G. [ID]; Scire, Jérémie; Yu, Hongjie; Wang, Wei; Cheng, Zhiyuan; Ducatez, Mariette F.; Stadler, Tanja [ID]

Bayesian phylodynamics reveals the transmission dynamics of avian influenza A(H7N9) virus at the human–live bird market interface in China

Claire Guinat[a,b,1] , Hao Tang[c] , Qiqi Yang[d] , Cecilia Valenzuela Agüí[a,b] , Timothy G. Vaughan[a,b] , Jérémie Scire[a,b] , Hongjie Yu[e], Wei Wang[e], Zhiyuan Chen[e], Mariette F. Ducatez[f] , and Tanja Stadler[a,b]

In 2013 to 2017, avian influenza A(H7N9) virus has caused five severe epidemic waves of human infections in China. The role of live bird markets (LBMs) in the transmission dynamics of H7N9 remains unclear. Using a Bayesian phylodynamic approach, we shed light on past H7N9 transmission events at the human–LBM interface that were not directly observed using case surveillance data-based approaches. Our results reveal concurrent circulation of H7N9 lineages in Yangtze and Pearl River Delta regions, with evidence of local transmission during each wave. Our results indicate that H7N9 circulated in humans and LBMs for weeks to months before being first detected. Our findings support the seasonality of H7N9 transmission and suggest a high number of underreported infections, particularly in LBMs. We provide evidence for differences in virus transmissibility between low and highly pathogenic H7N9. We demonstrate a regional spatial structure for the spread of H7N9 among LBMs, highlighting the importance of further investigating the role of local live poultry trade in virus transmission. Our results provide estimates of avian influenza virus (AIV) transmission at the LBM level, providing a unique opportunity to better prepare surveillance plans at LBMs for response to future AIV epidemics.

Phylodynamics | avian influenza | live bird markets | transmission | spill-over

Since its emergence in March 2013, avian influenza A(H7N9) virus has caused five epidemic waves of human infections in mainland China. A total of 1,568 laboratory-confirmed H7N9 human infections with 616 deaths were reported as of August 2020 (1), outreaching those globally caused by avian influenza A(H5N1) virus (n = 868) (2, 3) (Fig. 1). In wave 1, the spatial range of H7N9 human cases was mainly restricted to the Yangtze River Delta region in eastern China and extended toward the Pearl River Delta region in southern China during waves 2-3 (4, 5). Wave 5 attracted global attention since it was marked by i) an increased number of human infections, ii) an expansion in the spatial distribution of human infections toward northern and western China, and iii) the emergence of highly pathogenic avian influenza H7N9 virus (4). Among novel avian influenza viruses (AIV) to date, H7N9 virus raised the highest level of concern in terms of pandemic potential (6, 7) and negative public health impact (8).

Live bird markets (LBMs) are common in eastern and southern China and serve as trade premises for the distribution and sale of live poultry, with birds generally being held for a short period of time before sale (9–11). The majority of species sold in LBMs are indigenous yellow-feather broilers, followed by spent hens and waterfowl (10). There are two types of LBMs: retail LBMs serve as a major source of food for both urban and rural populations, while wholesale LBMs play a specialized role in the distribution of poultry in their areas and others (10, 12). However, the size and characteristics of each LBM, as well as the types of bird species sold, can vary greatly and lead to variations in the trade patterns and movements of poultry (12, 13). LBMs can be either indoor or outdoor facilities, with the majority being outdoors with the shed covering the stalls.

Exposure to infected poultry at LBMs was shown to be the major risk factor for H7N9 human infections. Of note, following confirmation of human infections, H7N9 viruses have been extensively detected in LBMs, mostly from chicken or environment samples (14). LBMs offer ideal environments for the emergence, maintenance, and dissemination of AIV with potential for zoonotic transmission (15, 16). This is because they combine a high density, turnover, and variety of bird species with a high contact frequency between birds and humans (9). Moreover, substantial and active live poultry trading through LBMs across the country increases the risk of AIV spread and human exposure (12, 13, 17, 18). Thus, continuous surveillance of AIV in LBMs is needed for emergence risk assessment and pandemic preparedness (19).

Significance

Our study used a phylodynamic model incorporating geographical and host structure to uncover critical information about the transmission dynamics of H7N9 virus in China including the number, geographic direction, and timing of new infections. By employing a Bayesian phylodynamic approach, we emphasize the significance of integrating epidemiological and genetic data to assess the epidemic state and inform future surveillance efforts for both public and animal health. Our findings highlight the importance of leveraging phylodynamic analyses to better understand and respond to emerging infectious diseases.

Given the critical role of LBMs in the spread of H7N9 viruses, various interventions were implemented at LBMs in most affected areas to respond to the epidemic (16, 20–22). In 2014, the Guangdong veterinary authority established the 1110 policy at LBMs, which involved daily cleaning, weekly disinfection, monthly rest day, and no overnight stay of poultry, and then, the Ministry of Agriculture and Rural Affairs (MARA) extended the policy to all provinces in February 2017 (23). Given the large number of human infections during wave 5 (Fig. 1), a national vaccination program for poultry was implemented in September 2017 (24). These measures together substantially reduced the intensity of H7N9 transmission in poultry and the number of human infections (20, 25–27). However, as novel H7N9 immune escape viruses emerged in China, the protective capacity induced by poultry vaccination might be no longer sufficient to protect humans from virus infection (28, 29), underlining the new threats that H7N9 viruses pose to human health.

Dynamic models of H7N9 transmission were developed to estimate the effective reproduction number R_e [defined as the average number of successful transmissions per infectious individual in a partially immune population at any time during an epidemic (30)] based on case surveillance data (31–40). R_e is an important parameter that reflects the level of disease transmissibility and is crucial to inform on the potential ease or difficulty in controlling disease transmission. Previous R_e estimates suggested a limited human-to-human transmissibility of H7N9 during the five epidemic waves, with R_e values far below 1 (32, 34, 36–40). To date, previous R_e estimates have only been inferred at the poultry level (32–34, 41), while control strategies for AIV in Asia are designed and implemented at the LBM level (18, 20, 27). Moreover, the limited quality of case surveillance data [due to reporting bias associated with the asymptomatic infections of H7N9 in poultry (42, 43)] together with outdated information on the poultry population sizes made it difficult to obtain realistic estimates of poultry-to-poultry and poultry-to-human transmissibility (31, 33, 35, 38).

Over the five epidemic waves from 2013 to 2017, H7N9 genome sequences from infected humans and poultry provide a unique opportunity to address the abovementioned shortcomings by quantifying the transmission dynamics of H7N9 viruses using phylodynamic approaches (44, 45). These approaches require the specification of a model that generates the sampled transmission tree underlying the epidemiological dynamics of disease transmission. Birth–death models are a class of such tree-generating models. Among other key properties, they directly provide estimates of epidemiological parameters of interest, notably R_e; they also explicitly account for the sampling intensity (46–49). Moreover, progress has been recently made to allow for the inference of incidence trajectories from these models (50). Here, we take advantage of such recent advances in phylodynamics to update and improve the estimates of key epidemiological parameters and transmission patterns of H7N9 at the human–LBM interface during the five epidemic waves in China (2013 to 2017) by providing records of past H7N9 transmission events that were not directly observed using case surveillance data-based approaches. In addition, we compare H7N9 transmissibility and surveillance intensity across epidemic waves, in particular between waves 1-4 and wave 5.

Results

Transmission Dynamics of H7N9 in China. To shed light on the transmission dynamics of H7N9 virus in China, we performed a Bayesian phylodynamic analysis of H7N9 genome sequences of the hemagglutinin (HA) gene segment collected from infected poultry at LBMs and infected humans in the Yangtze and Pearl River Delta regions during the five epidemic waves in China. We fitted a multitype birth–death (MTBD) model to the aligned sequences to simultaneously infer key epidemiological parameters (i.e., effective reproductive number R_e, infectious period, and sampling proportion) and phylogenetic trees (51). Since the first H7N9 human cases were reported in the Yangtze River Delta region and the viruses sampled from this first group of cases were identified as of being of avian origin (52, 53), we assumed LBMs in the Yangtze River Delta region as the subpopulation (deme) of epidemic origin. Moreover, since the human-to-human transmissibility of H7N9 remained very limited over the five waves (35, 54, 55), we assumed that the human cases were generated via exposure to infected poultry at LBMs, meaning that the transmission of H7N9 to humans only occurs at the tips of
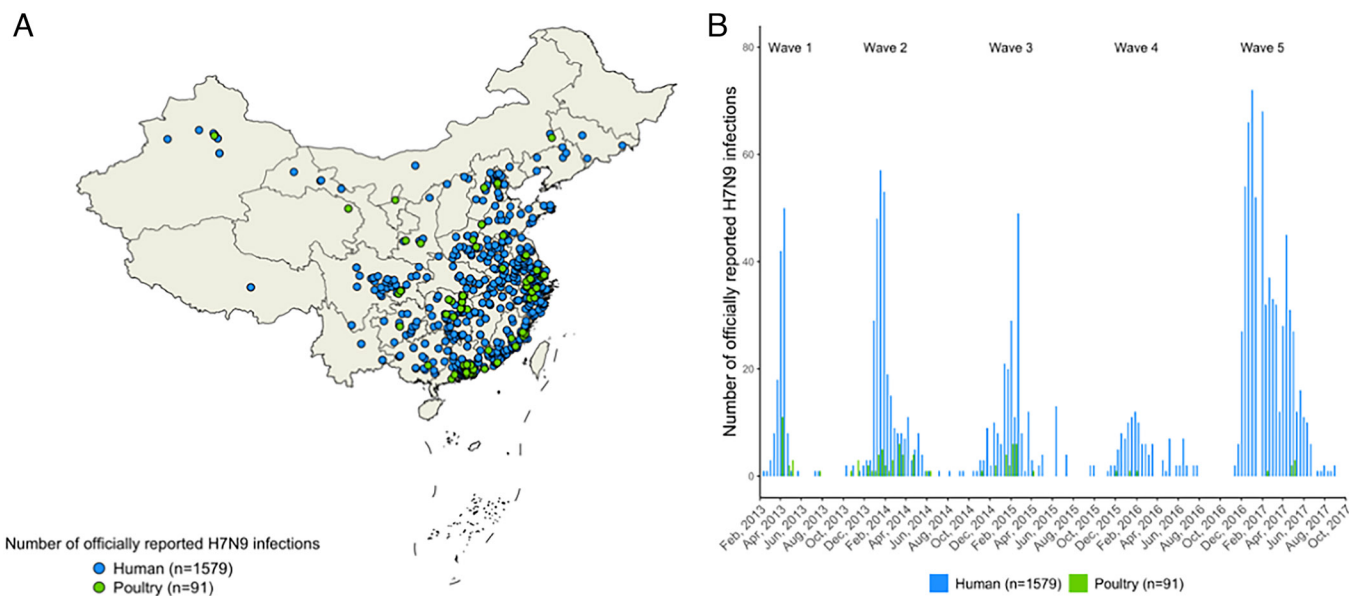

Fig. 1. Spatial (*A*) and temporal (*B*) distribution of the number of officially reported human and poultry infections of avian influenza A(H7N9) virus during the five epidemic waves in China (2013 to 2017).

the phylogenetic trees and originates from LBMs. The resulting maximum clade credibility (MCC) tree (Fig. 2) shows that the Yangtze River Delta region was host to a wide range of H7N9 lineages but also exhibited lineage movements to the Pearl River Delta region. From wave 2, several lineages appeared to have been circulating at the same time in both regions. During each wave,
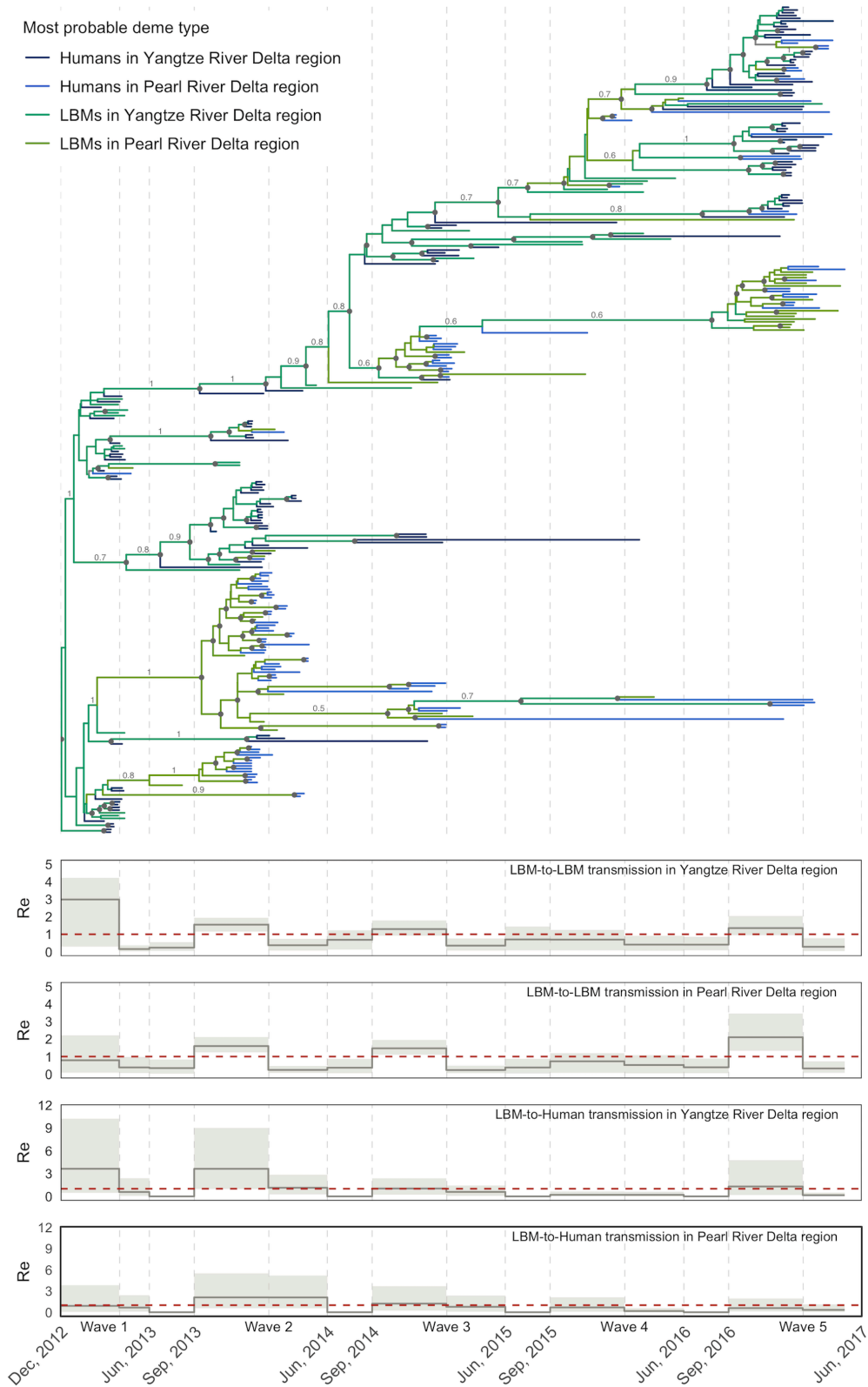
Fig. 2. Maximum clade credibility (MCC) tree estimated from H7N9 genome sequences of the hemagglutinin (HA) gene segment collected between 1st February 2013 and 30th April 2017 in China. Branch colors indicate the most probable deme type. Circles at internal nodes indicate clade posterior probabilities above 0.75. For selected nodes, numbers show the posterior probabilities of the most probable deme type. Effective reproduction numbers (R_e) through time, simultaneously inferred with the phylogenetic trees of the H7N9 genome sequences, using the multitype birth–death model. The dark gray line and the light gray shading represent the median posterior estimate of R_e and the 95% highest posterior density credible intervals, respectively. The red dashed line represents the threshold 1. The vertical dashed gray lines represent the 14-time intervals for R_e estimations.

local transmission of lineages was observed within each region. The estimated time to the most recent common ancestor (tMRCA) of H7N9 genome sequences of the HA gene segment was estimated at the end of December 2012 (median: 27 December 2012, 95% highest posterior density credible intervals (HPD): 18 November 2012 to 22 January 2013) (*SI Appendix*, Table S1).

To assess whether H7N9 transmissibility changed across waves, we inferred key epidemiological parameters across different time intervals. R_e was inferred across 14-time intervals and showed a seasonal increase with five periods of growth (Fig. 2), coinciding with the five epidemic waves (Fig. 1). Only the following R_e estimates were significantly above 1 in the time interval from beginning of September to end of January (Fig. 2 and *SI Appendix*, Table S1): R_e between LBMs in the Yangtze Delta River region in wave 2 (median: 1.5, 95% HPD: 1.2 to 1.9); R_e between LBMs in the Pearl Delta River region in waves 2 (median: 1.6, 95% HPD: 1.2 to 2.1), 3 (median: 1.5, 95% HPD: 1.1 to 1.9), and 5 (median: 2.1, 95% HPD: 1.3 to 3.5); and R_e from LBMs to humans in the Yangtze Delta River region in wave 2 (median: 3.6, 95% HPD: 1.0 to 9.0). From the corresponding sequences, no molecular markers were found associated with a putative increase in the R_e estimates. Most R_e estimates from LBMs in the Yangtze Delta River region to LBMs in the Pearl Delta River region (and vice versa) were significantly below 1 during the five waves, with only a few 95% HPD intervals including 1 (*SI Appendix*, Fig. S1 and Table S1). The infectious period was inferred across two-time intervals corresponding to the start of wave 5 (Fig. 3 and *SI Appendix*, Table S1). The median infectious period for humans (i.e., time from infection to recovery or death of an infected individual)

during waves 1-4 was estimated to be 9 d (95% HPD: 3 to 14) in the Yangtze Delta River region and 6 d (95% HPD: 2 to 11) in the Pearl Delta River region. In wave 5, a significantly longer median infectious period was inferred in the Yangtze Delta River region (median: 11 d, 95% HPD: 4 to 19) ($P < 0.001$) and in the Pearl Delta River region (median: 12 d, 95% HPD: 2 to 29) ($P < 0.001$). The median infectious period for LBMs (i.e., time from infection to depopulation and cleaning/disinfection of an infected LBM) during waves 1-4 was estimated to be 44 d (95% HPD: 29 to 64) in the Yangtze Delta River region and 23 d (95% HPD: 13 to 39) in the Pearl Delta River region. In wave 5, a significantly shorter median infectious period was inferred in the Yangtze Delta River region (median: 32 d, 95% HPD: 10 to 66) ($P < 0.001$), while it was significantly longer in the Pearl Delta River region (median: 60 d, 95% HPD: 22 to 114) ($P < 0.001$). The inferred sampling proportion can be found in *SI Appendix*, Table S1.

Timeline of the First H7N9 Infections in China. To explore the timing of the first H7N9 infections in China, we inferred the date of the first infection per subpopulation (deme) from the posterior epidemiological parameters and phylogenetic trees (50) and compared them with the date of the first officially reported infection (Fig. 4 and *SI Appendix*, Table S2). The first human case in the Yangtze Delta River region (median: 19 December 2012, 95% HPD: 29 October 2012 to 23 January 2013) occurred 8.9 wk earlier than the officially reported one (19 February 2013). Similarly, a 10.1-wk difference was observed between the inferred (median: 2 February 2013, 95% HPD: 15 December 2012 to 11 April 2013) and the date of the first officially reported human case
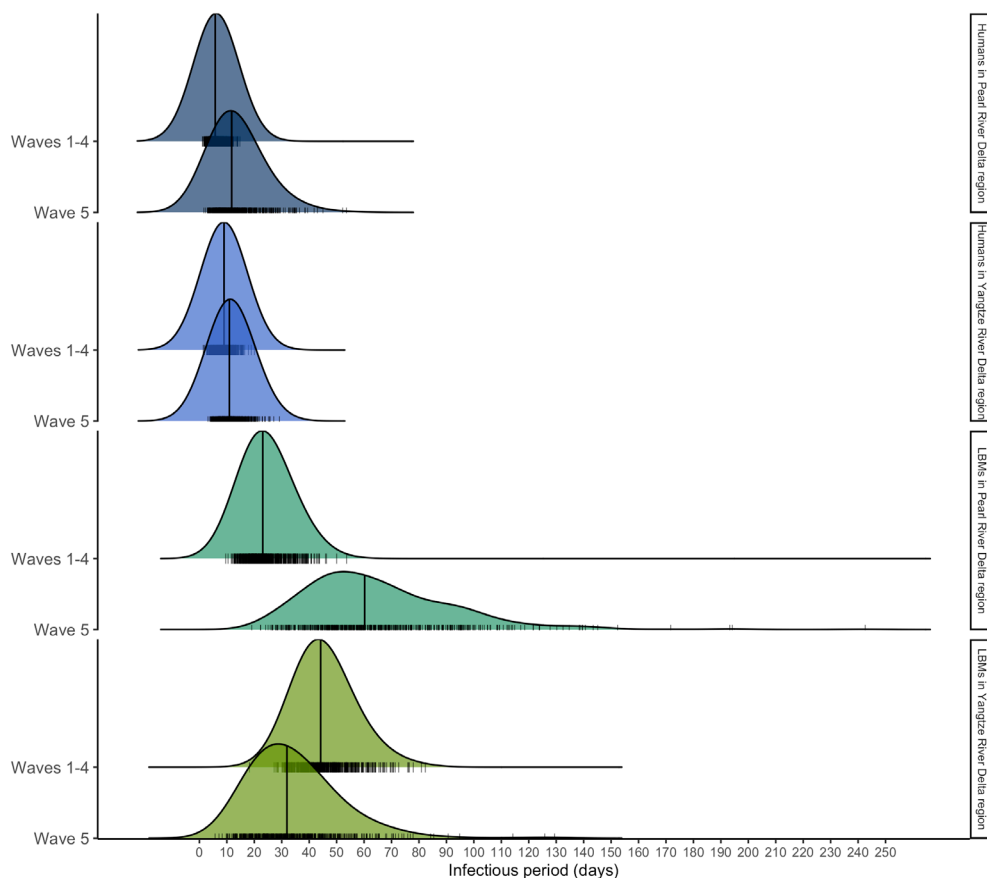
Fig. 3. Posterior distributions of the infectious period (in days) per deme across two-time intervals (waves 1-4 and wave 5), corresponding to the start of the fifth epidemic wave, inferred by the multitype birth–death model. The black vertical line represents the median estimates of the infectious period. The black vertical lines along the *X* axis represent the estimates of the infectious period from which the density distributions are generated.
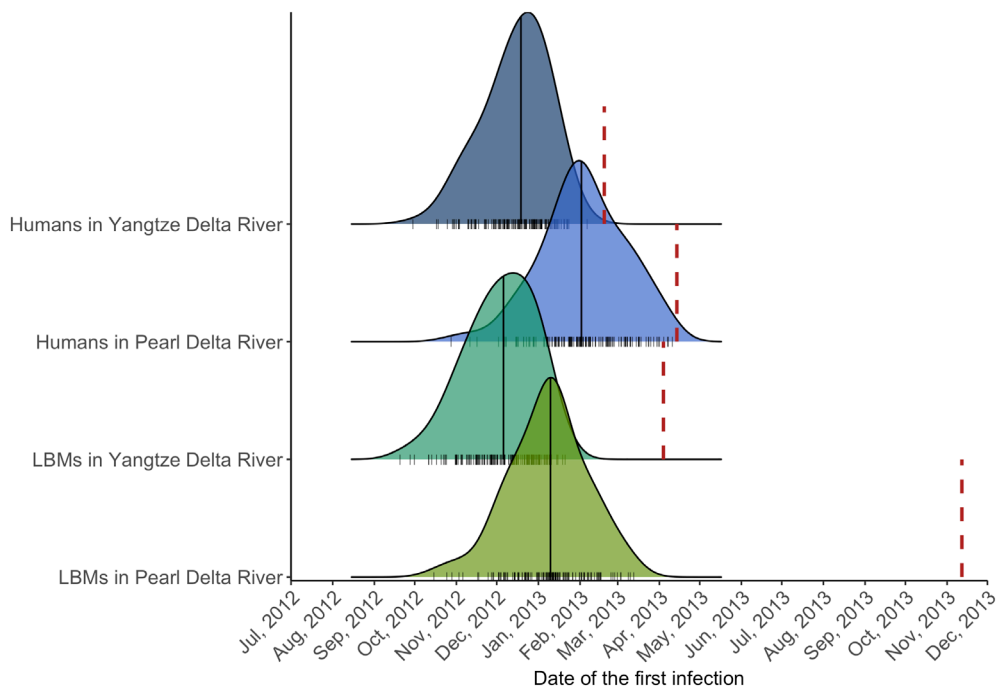
Fig. 4. Posterior distribution dates of the first infection in each deme inferred from the posterior epidemiological parameters and phylogenetic trees. The black vertical line represents the median date. The black vertical lines along the *X* axis represent the date estimates from which the density distributions are generated. The vertical red dashed line represents the date of the first officially reported infection in each deme.

in the Pearl Delta River region (14 April 2013). The first LBM outbreak in the Yangtze Delta River region (median: 6 December 2012, 95% HPD: 10 Oct 2012 to 11 January 2013) occurred 16.9 wk earlier than the officially reported one (4 April 2013). A longer difference (43.7 wk) was observed between the inferred (median: 10 January 2013, 95% HPD: 25 November 2012 to 12 March 2013) and the date of the first officially reported LBM outbreak in the Pearl Delta River region (12 November 2013).

Role of LBMs in H7N9 Virus Spread in China. To disentangle the role of LBMs in the spread of H7N9, we inferred the median number of new infections per subpopulation (deme) and per month from the posterior epidemiological parameters and phylogenetic trees (50) and compared them with the number of officially reported infections (56) (Fig. 5). We inferred five epidemic waves, that exhibited seasonal cycles, in which human cases and LBM outbreaks occurred during winter and peaked in January. We showed that only human cases and LBM outbreaks in the Yangtze Delta River region occurred in wave 1, with a peak of 350 LBM outbreaks (95% HPD: 10 to 1,280) and 480 human cases (95% HPD: 82 to 1,707) in March 2013. During wave 2, a drastic increase in the number of human cases and LBM outbreaks was observed in the Pearl Delta River region, outreaching those estimated in the Yangtze Delta River region. A peak was observed in January 2014, with a median of 409 LBM outbreaks (95% HPD: 178 to 1,045) and 613 human cases (95% HPD: 123 to 1,543) in the Pearl Delta River region. From wave 2 to wave 4, the median number of infections substantially decreased in all demes. During wave 5, the median number of infections increased again, reaching in January 2017 up to 230 LBM outbreaks (95% HPD: 48 to 4,968) and 266 human cases (95% HPD: 42 to 4,594) in the Yangtze Delta River region and up to 732 LBM outbreaks (95% HPD: 26 to 113,300) and 233 human cases (95% HPD: 20 to 16,635) in the Pearl Delta River region.

Over the five epidemic waves, we inferred a median of 2,915 (95% HPD: 517 to 18,328) and 3,588 (95% HPD: 539 to 47,295) human cases in Yangtze and Pearl Delta River regions,

respectively, outreaching the officially reported numbers, i.e., 728 and 384 human cases (56). We inferred a median of 2,448 LBM outbreaks (95% HPD: 383 to 18,641) in the Yangtze Delta River region due to transmission from LBMs in the same region and 615 (95% HPD: 22 to 24,543) due to transmission from LBMs in the Pearl Delta River region, while only 19 LBM outbreaks have been officially reported (56). We inferred a median of 3,075 LBM outbreaks (95% HPD: 478 to 161,751) in the Pearl Delta River region due to transmission from LBMs in the same region and 583 (95% HPD: 24 to 8,930) due to transmission from LBMs in the Yangtze Delta River region, while only 39 LBM outbreaks have been officially reported (56).

Discussion

This study employed a Bayesian phylodynamic approach to investigate the transmission dynamics of H7N9 virus at the human–LBM interface in China. By analyzing genome sequences, we provide detailed insights into the virus spatiotemporal movements across the Yangtze and Pearl Delta River regions. Our results revealed that the Yangtze River Delta region hosted a diverse range of H7N9 lineages, with some moving to the Pearl River Delta region. Concurrent circulation of lineages was observed in both regions, with evidence of local transmission during each wave. While the resulting MCC tree was consistent with prior studies (57, 58), our approach is unique in using MTBD models for the phylodynamic analyses. Discrete trait approaches have been often used to investigate the transmission dynamics of AIV (57–60) among different host types due to their computational efficiency and ease of implementation, but MTBD models have several advantages. They can account for complex demographic and epidemiological processes, including transmission, removal, and sampling of lineages, providing more accurate insights into disease transmission dynamics. Moreover, MTBD models integrate the sampling proportion, making them more robust to potential sampling biases, and can directly estimate critical parameters, such as
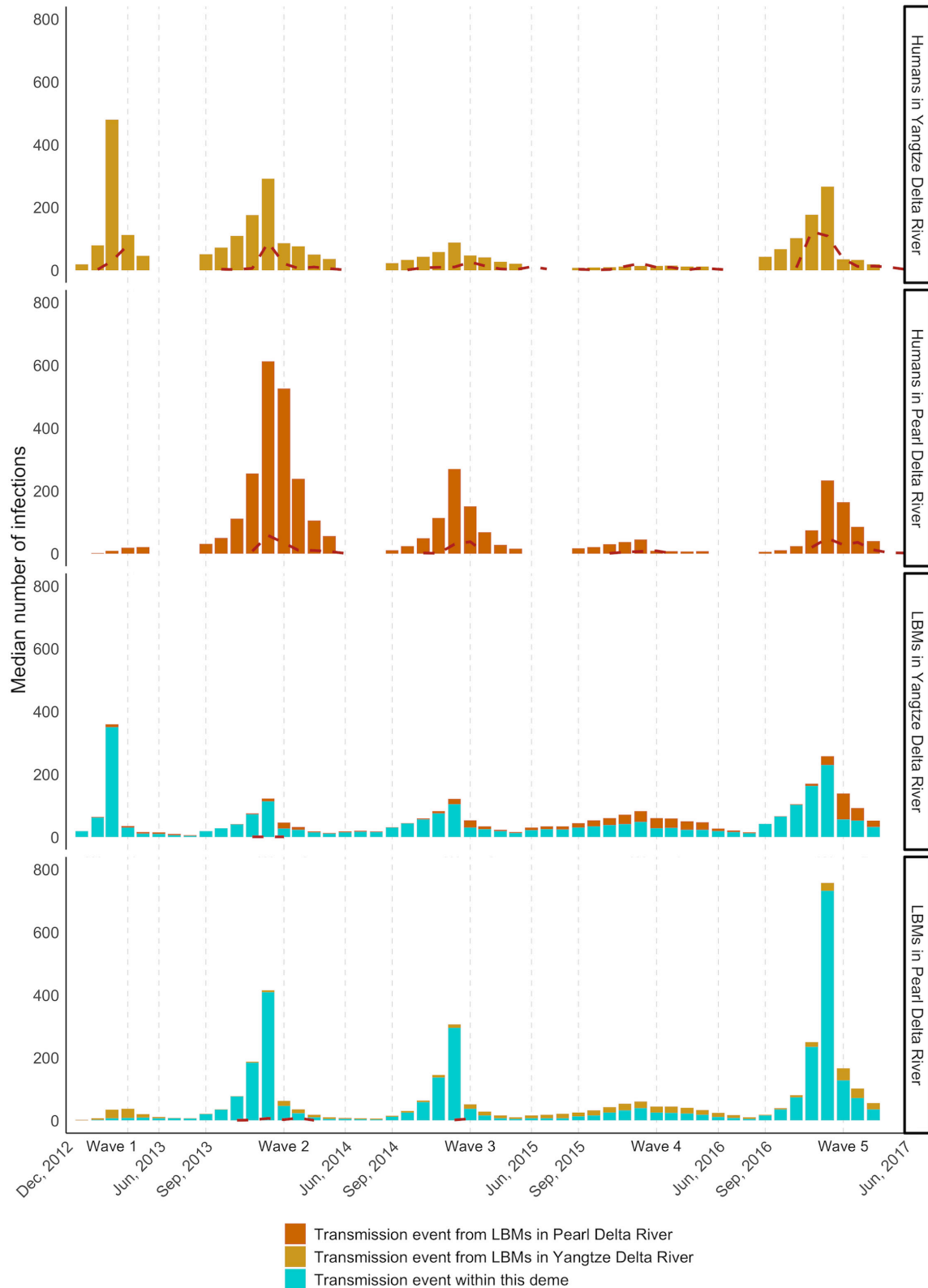
Fig. 5. Median number of infections per month for each deme inferred from the posterior epidemiological parameters and phylogenetic trees. The yellow bars represent those caused by transmission events from LBMs in the Yangtze Delta River, the orange bars represent those caused by transmission events from LBMs in the Pearl Delta River, and the blue bars represent those due to transmission events within the given deme. The black dashed line represents the number of officially reported infections per month for each deme.

the effective reproductive number (R_e), which can inform health interventions. Finally, we allow for the estimation of incidence trajectories, providing critical information for understanding the spatiotemporal dynamics of virus transmission.

Our findings suggest that the H7N9 virus had circulated undetected in humans and LBMs for several weeks to several months before its first official identification in Yangtze and Pearl Delta River regions, corroborating previous reports of undetected H7N9

spread in China (42, 43). We were able to quantify the seasonality of H7N9 transmission in China based on H7N9 genome sequences. So far, this seasonal trend had been observed from the human case surveillance data and had been difficult to quantify due to underreporting associated with the asymptomatic infections of H7N9 in poultry (42, 43). The incidence trajectories followed the same temporal dynamics of the officially reported infections and suggested a large number of unreported or undetected infections in both regions, in particular in the LBM demes. During waves 1-4, the circulating H7N9 viruses were of low pathogenicity to poultry and did not cause any symptoms in infected poultry, allowing the virus to silently spread among poultry (42, 61). Consequently, it was difficult to identify infected poultry and associated human infections, explaining why the number of officially reported infections was likely underestimated. The estimates we inferred could inform the LBM census data in China, which are currently unavailable. As an example, in 2014, the number of active LBMs was estimated at 1,877 in the Yangtze Delta River region and at 1,210 in the Pearl Delta River region by combining four sources of data (62). Our estimates suggest that a higher number of LBMs might be active in the country, supported by the fact that some LBMs may not be registered with the government. Our study provides estimates of R_e for H7N9 virus spread at the human–LBM interface, providing a unique opportunity to better prepare surveillance plans at LBMs for response to AIV outbreaks. So far, these estimates were only available at the poultry level (32–34, 41), while control strategies for AIV in Asia are designed and implemented at the LBM level (18, 20, 27). Thus, these epidemiological parameters will improve our ability to provide predictions of virus spread at the human–LBM interface for the development of strategies for the long-term control of AIV epidemics.

Our study indicates that the transmission of H7N9 virus between LBMs was more likely to occur within regions (i.e., over short distances and between provinces in close proximity), such as within the Yangtze Delta River and the Pearl Delta River regions. This regional structure of transmission was evidenced by the high rates of transmission and number of simulated infections within these regions. This finding is consistent with previous studies that identified a regional spatial structure for the spread of H7N9 virus (59) and live poultry movements (12), highlighting the importance of further investigating the role of local live poultry trade in virus transmission. The absence of available genome sequences from the intermediate provinces linking the two regions (Jiangxi, Fujian, and Hubei) means that, despite being limited, transmission events between the two regions could have occurred over short distances. Given these results, prevention and control efforts for H7N9 should consider the regional structure of transmission in their strategies.

Our study aimed to assess the differences in the transmissibility of H7N9 virus by considering the distinct waves and estimating the parameters of the infectious period and sampling proportion separately. Nonetheless, the restricted availability of genome sequences hindered the full differentiation of highly pathogenic (HP) and low pathogenic (LP) H7N9 in wave 5, thus limiting our capability to derive conclusive results. Nevertheless, the data provided some evidence of the variation in transmissibility between HP and LP H7N9. During wave 5, the transmission of H7N9 between LBMs in the Pearl Delta River was observed as particularly high, with a median R_e estimate of 2.2 and a peak in LBM outbreaks in January 2017 with a median of 732. This trend, coupled with the dominance of HP H7N9 in the region (63), suggests a higher transmissibility of HP H7N9 compared to LP H7N9, consistent with previous experimental studies (64). Furthermore, infected humans in the Pearl River Delta region

during wave 5 were found to be infectious for a longer period compared to waves 1-4 (median 12 vs. 6 d), which could be attributed to reduced health care resources and decreased capacity for early identification and hospitalization of infected individuals, particularly in rural areas where HP H7N9 human infections were more prevalent (65). LBMs in the Pearl River Delta region also exhibited a longer infectious period compared to waves 1-4 (median 60 vs. 23 d), which may indicate greater adaptation of HP H7N9 to the poultry and environment in the region or differences in the control strategies implemented at LBMs between the two regions. Previous epidemiological studies have estimated a similar range of infectious periods for humans during waves 1-3 (ranging from 13 to 21 d) (34, 66, 67). In accordance with our findings, one epidemiological study reported a longer time from illness onset to death for HP H7N9 human cases compared to LP H7N9 cases (median 31 vs. 16 d) (68). However, it is important to note that these epidemiological studies may suffer from reporting bias, such as underdetection of mild illness which may lead to biases in the estimations, unlike the phylodynamic approaches employed in our study.

The proposed Bayesian phylodynamic model focuses on the predominant routes of transmission of the H7N9 virus, including inter-LBM transmission and LBM–human transmission. The model does not take into consideration the potential contribution of migratory wild birds and poultry farms to the introduction of the virus (69, 70). Although some studies have demonstrated that experimentally infected songbirds and parakeets can shed the virus and that tree sparrows were tested positive during surveillance campaigns (71, 72), the role of wild birds in H7N9 transmission is still not well understood. However, some evidence suggests that migratory wild birds may play a minor role due to the adaptation of H7N9 virus to gallinaceous poultry rather than duck and geese (42). Wild bird migration was also not associated with the spatial spread of H7N9 virus (59). Additionally, the recurring human cases during the winter months are believed to be associated with seasonality in poultry production and consumption in China, such as an increase in trade during the Lunar New Year celebration, when people are more likely to consume more chickens (73, 74) rather than seasonal migrations of wild birds. The majority of H7N9 viruses have been isolated from LBMs, rather than poultry farms, and very few human cases have been associated with infected poultry farms (68, 75). These data suggest that LBMs, rather than poultry farms, were the origin of the novel H7N9 viruses. Although consumers primarily purchase live poultry at retail LBMs [i.e., LBMs where live poultry is sold to consumers (10, 12)], the virus could circulate among different types of LBMs that are interconnected along the live poultry value chain (10, 12). However, due to data limitation, it was not possible to obtain information on the size and characteristics of the LBMs from which the H7N9 genome sequences were sampled, including the types of birds sold, indoor/outdoor setting, and retail/wholesale [i.e., LBMs where live poultry is sold to wholesalers and retailers (10, 12)], which could result in differences in disease transmission dynamics (13, 76) and hinder the assessment of differences in H7N9 transmission among different types of LBMs. Additionally, the limited number of H7N9 genome sequences from LBMs resulted in wide credible intervals for the R_e estimates. Thus, further surveillance efforts should include more intensive virus sampling in various poultry premises.

In summary, our study provides important insights into the transmission dynamics of the H7N9 virus at the human–LBM interface in China. Despite the vaccination campaign, the virus persists in spreading within the country (28, 29). Therefore, it is crucial to conduct further surveillance studies of both poultry and

wild bird populations to monitor the geographic distribution and expansion of the virus. By doing so, we can enhance our preparedness and response to future AIV epidemics.

Methods

Selection and Alignment of H7N9 Genome Sequences. We downloaded all H7N9 genome sequences of the HA gene segment, that were collected between 1st February 2013 and 30th April 2017 in China, from the GISAID database (Global Initiative on Sharing All Influenza Data, http://www.gisaid.org) on 1st September 2021. Sequences were selected if they were coming from humans or LBMs in the Yangtze River Delta region (including Anhui, Jiangsu, Shanghai, and Zhejiang provinces) and the Pearl River Delta region (including Guangdong, Guangxi and Hunan provinces) and were associated with a complete sampling date. Information about the LBM identifiers was shared by the submitting laboratory (Harbin Veterinary Research Institute, China). The resulting alignment of 798 sequences was made using MAFFT v7 (77) and checked using AliView v1.26 (78). Sequences with insertion of multiple basic amino acids in the HA cleavage site were labeled as Highly Pathogenic (79), while the remaining were identified as Low Pathogenic. In 10 out of 62 LBMs (16.1%), multiple sequences were obtained from infected birds sampled on the same day and showed high genetical similarity (98.6 to 99.0%); we thus performed a random subsampling procedure to select only one representative sequence per LBM. To render the phylodynamic analysis computational feasible, we also randomly subsampled the set of human sequences to obtain a final set of 300 genome sequences. Selected sequences were annotated with available sampling dates (between 27st February 2013 and 27th April 2017), geographical locations (Yangtze or Pearl River Delta region), and host types (human or LBM). The final set consisted of 238 sequences from human cases and 62 sequences from LBM outbreaks (Fig. 6 and *SI Appendix*, Table S3).

Phylodynamic Inference of H7N9 Transmission Dynamics. Bayesian phylodynamic analyses were implemented using the *BDMM-Prime* package for BEAST v2.6.3 (80) and the BEAGLE library (80) to improve computational performance. The MTBD model was used as the tree prior (81, 82). Similar to compartmental models in epidemiology, the MTBD model assumes that the underlying population is structured into discrete subpopulations (or demes), each with specific transmission, removal, and sampling rates and allows inference of the effective reproductive number R_e directly from genome sequences. Under this model, demes were defined according to host type and geographical location of genome sequences: humans in the Yangtze River Delta region, humans in the Pearl River Delta region, LBMs in the Yangtze River Delta region, and LBMs in the Pearl

River Delta region (*SI Appendix*, Table S3). We assumed that infected LBMs in Yangtze and Pearl River regions could transmit the virus to i) other LBMs through trade-related movements of infected birds or contaminated fomites (LBM-to-LBM R_e, defined as the number of secondary infected LBMs caused by one infectious LBM) (13, 83) or ii) to humans through exposure to infected birds (LBM-to-human R_e, defined as the number of secondary infected humans caused by a given infectious LBM) (16, 20, 84, 85) (*SI Appendix*, Fig. S4). Given that most households frequently purchase poultry at local LBMs (9), we assumed that infected LBMs could not transmit the virus to humans located in another region. Given that most human cases were likely due to exposure to infected birds at LBMs (16, 20, 84, 85) and the limited human-to-human transmissibility of H7N9 inferred over the five epidemic waves (35, 54, 55), we assumed that infected humans could not transmit the virus to other humans. Infected humans were considered noninfectious following recovery or death (with a becoming noninfectious rate δ_{human}) and were sampled and sequenced with a sampling proportion S_{human}. Infected LBMs were considered noninfectious following depopulation and cleaning/disinfection measures (with a becoming noninfectious rate δ_{LBM}) and were sampled and sequenced with a sampling proportion S_{LBM}.

The MTBD model was combined with a HKY + Γ_4 nucleotide substitution model (86, 87), a relaxed molecular clock model (88) defined by a lognormal(0.001,1.25) prior distribution, corresponding to a median of 4×10^{-4} substitution per site per year (95% interquartile range (IQR): 3×10^{-5} to 5×10^{-3}) (87, 89). The origin of the tree was associated with the deme LBMs in the Yangtze River Delta since the H7N9 virus likely emerged from this region (from Jiangsu and Zhejiang provinces), and the viruses sampled from the first human cases were identified as of avian origin (52, 53). The origin of the tree was given a lognormal(1.5, 0.05) prior distribution corresponding to a median date 23th October 2012 (95% IQR: 8th May 2012 to 25th March 2013) (90). The become noninfectious rate of humans was given a lognormal(36, 0.6) prior distribution corresponding to a median infectious period of 10 d (95% IQR: 3.7 to 39.2) (4, 34, 66, 67, 91). Given the lack of information, the become noninfectious rate of LBMs was given a broader prior distribution [lognormal(24, 0.6)] corresponding to a median infectious period of 15 d (95% IQR: 5.6 to 58.5). For each deme, the sampling proportion was given a uniform prior distribution, with the upper bound informed by the number of H7N9 genome sequences and the reported number of human cases and LBM outbreaks (56). Given the lack of information on the transmissibility of H7N9 from LBMs to LBMs and from LBMs to humans, the LBM-to-LBM and LBM-to-human R_e parameters were given a broad prior distribution [lognormal(0,1)] corresponding to a median 1 (95% IQR: 0.1 to 7.1). More information on the prior values and distributions of the model parameters can be found in *SI Appendix*, Table S4.
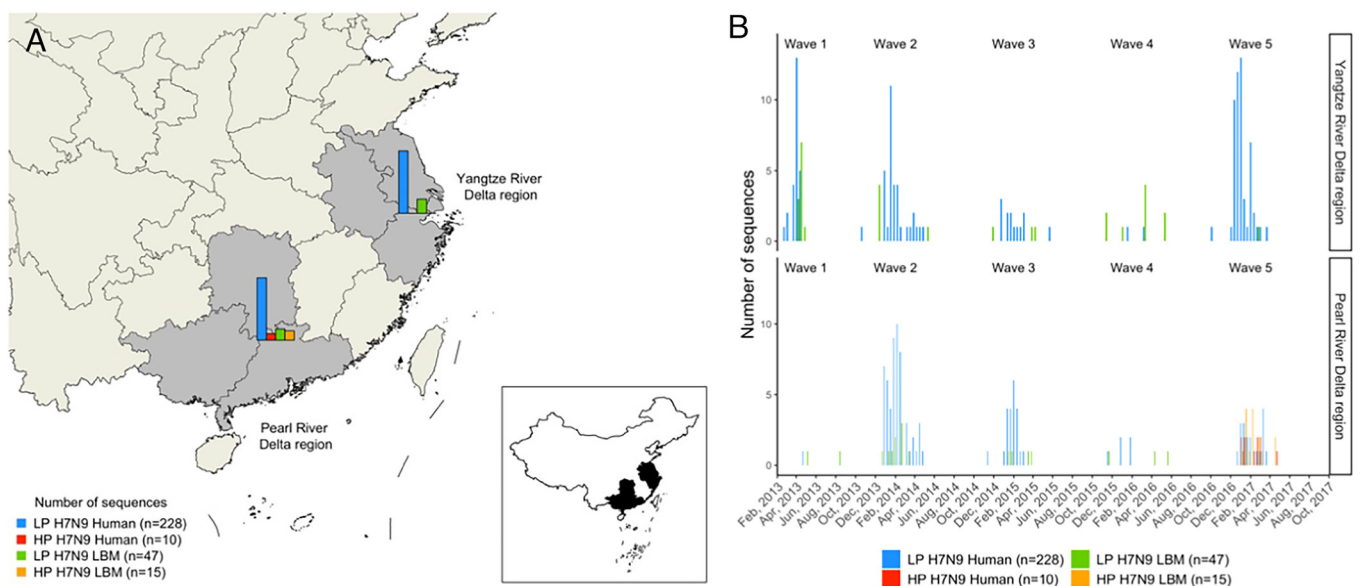

Fig. 6. Spatial (*A*) and temporal (*B*) distribution of H7N9 genome sequences of the hemagglutinin (HA) gene segment from human cases and LBM outbreaks in the Yangtze and Pearl River Delta regions in China, 2013 to 2017. Sequences with insertion of multiple basic amino acids in the HA cleavage site were labeled as Highly Pathogenic (HP), while the remaining were identified as Low Pathogenic (LP).

All parameters were assumed to be deme specific and were estimated across different time intervals. To evaluate differences in infectiousness duration and account for variations in sampling rates between waves 1-4 and wave 5, the become noninfectious rate and the sampling proportion parameters were estimated across two-time intervals corresponding to waves 1-4 (from January 2013 to August 2016) and wave 5 (from September 2016 to April 2017). To evaluate differences in transmissibility of H7N9 virus between waves, the R_e parameters were estimated across 14-time intervals corresponding to the changes in the number of cases, including periods of increasing, decreasing, and limited case numbers (Fig. 1). For each time interval, association between increased R_e estimates and amino acid substitution in the corresponding sequences was carried out using AliView v1.26 (78).

Posterior estimates of model parameters were inferred using Markov chain Monte Carlo (MCMC). All analyses were run for 100 million steps across five independent Markov chains (MCMC), and states were sampled every 10,000 steps. The first 10% of steps from each analysis were discarded as burn-in before states from the chains were pooled using Log-Combiner v2.6.3 (92). Convergence was assessed in Tracer v1.7 (93) by ensuring that the estimated sampling size values associated with the posterior model parameters were all >200. Posterior multitype phylogenetic trees (i.e., phylogenetic trees that are associated with a specific deme along their branches) were inferred from a subsampled set of posterior phylogenetic trees and model parameters (n = 500) using a stochastic mapping algorithm (51, 94). The MCC tree was obtained from the multitype phylogenetic trees in TreeAnnotator v2.6.3 (92) and annotated using the *ggtree* package (95) in R v4.0.2 (96). Incidence trajectories (i.e., the number of newly infected hosts per deme over time due to within-deme and between-deme transmission) were inferred from a subsampled set of posterior phylogenetic trees and model parameters (n = 500) using a particle filtering algorithm (50).

To test the robustness of the phylodynamic analysis with respect to changes in the priors' assumptions, a separate set of analyses were performed by using a broader prior for the within- and between-deme R_e parameters [lognormal(1,1), corresponding to a median of 2.7 (95% IQR: 0.4 to 19.3)] (*SI Appendix*, Fig. S5), as well as by reperforming the random subsampling procedures of bird and human sequences (*SI Appendix*, Fig. S6), which did not significantly change the temporal dynamics of the R_e estimates (<1 and >1) compared to the main analysis.

Data, Materials, and Software Availability. All H7N9 genome sequences of the HA gene segment used in this study are available on the GISAID database (http://www.gisaid.org) (97). Case surveillance data shown in this study are available on the FAO database (Food and Agriculture Organization of the United Nations, https://empres-i.apps.fao.org) (98). The prior values and distributions of the model parameters are described in *SI Appendix*, Table S5. The BEAST 2 XML file used to perform the phylodynamic analysis together with the accession numbers of the H7N9 genome sequences, and the R scripts are available at https://github.com/ClaireGuinat/h7n9_bdmm-prime (99).

Author affiliations: ªDepartment of Biosystems Science and Engineering, ETH Zürich, 4058 Basel, Switzerland; ᵇSwiss Institute of Bioinformatics, 1015 Lausanne, Switzerland; ᶜCentre for Biosecurity and One Health, Harry Butler Institute, Murdoch University, Murdoch, WA 6150, Australia; ᵈDepartment of Ecology and Evolutionary Biology, Princeton University, Princeton, NJ 08544; ᵉSchool of Public Health, Fudan University, Key Laboratory of Public Health Safety, Ministry of Education, 200032 Shanghai, China; and ᶠUnit of Host-Pathogens Interactions, University of Toulouse, National Research Institute for Agriculture, Food and the Environment, National Veterinary School of Toulouse, 31300 Toulouse, France

1. FAO, H7N9 situation update August 2020 (2017). Available at: http://www.fao.org/ag/againfo/programmes/en/empres/H7N9/situation_update.html (Accessed 12 January 2022).
2. R. J. Webby, Z. Yang, The changing landscape of A H7N9 influenza virus infections in China. *Lancet. Infect. Dis.* **17**, 783–784 (2017).
3. WHO, Cumulative number of confirmed human cases of avian influenza A(H5N1) reported to WHO. Available at: https://cdn.who.int/media/docs/default-source/influenza/human-animal-interface-risk-assessments/2022_nov_tableh5n1.pdf?sfvrsn=babfcad1_1&download=true (Accessed 12 January 2022).
4. S. Su *et al.*, Epidemiology, evolution, and pathogenesis of H7N9 influenza viruses in five epidemic waves since 2013 in China. *Trends Microbiol.* **25**, 713–728 (2017).
5. T.T.-Y. Lam *et al.*, Dissemination, divergence and establishment of H7N9 influenza viruses in China. *Nature* **522**, 102–105 (2015).
6. Z. Pu *et al.*, Potential pandemic of H7N9 avian influenza A virus in human. *Front. Cell Infect. Microbiol.* **8**, 414 (2018).
7. J. Shi *et al.*, H7N9 virulent mutants detected in chickens in China pose an increased threat to humans. *Cell Res.* **27**, 1409–1421 (2017).
8. CDC, Influenza risk assessment tool (IRAT) (2021). Available at: https://www.cdc.gov/flu/pandemic-resources/national-strategy/risk-assessment.htm (Accessed 12 January 2022).
9. Q. Liao, W. T. Lam, G. M. Leung, C. Jiang, R. Fielding, Live poultry exposure, Guangzhou, China, 2006. *Epidemics* **1**, 207–212 (2009).
10. H. Tang *et al.*, Value chain analysis of yellow broiler industry in Guangxi, China to inform H7N9 influenza control strategies. *Prev. Vet. Med.* **190**, 105328 (2021).
11. X. Zhou *et al.*, Knowledge, attitudes, and practices associated with avian influenza along the live chicken market chains in Eastern China: A cross-sectional survey in Shanghai, Anhui, and Jiangsu. *Transboundary Emerg. Dis.* **66**, 1529–1538 (2019).
12. H. Tang *et al.*, Analysis of the movement of live broilers in Guangxi China and implications for avian influenza control. *Transboundary Emerg. Dis.* **69**, e775–e787 (2021).
13. X. Zhou *et al.*, The role of live poultry movement and live bird market biosecurity in the epidemiology of influenza A (H7N9): A cross-sectional observational study in four eastern China provinces. *J. Infect.* **71**, 470–479 (2015).
14. M. Kang *et al.*, Environmental sampling for Avian Influenza A(H7N9) in live-poultry markets in Guangdong, China. *PLoS One* **10**, e0126335 (2015).
15. P. Zhou *et al.*, Avian influenza A (H7N9) virus and mixed live poultry–animal markets in Guangdong province: A perfect storm in the making? *Emerging Microbes Infect.* **4**, 1–3 (2015).
16. C. Bao *et al.*, Live-animal markets and influenza A (H7N9) virus infection. *N. Engl. J. Med.* **368**, 2337–2339 (2013).
17. W. Liu *et al.*, Spatial and temporal analysis of human infection with avian influenza A (H7N9) virus in China, 2013. *Eurosurveillance* **18**, 20640 (2013).
18. Y. Li *et al.*, Closure of live bird markets leads to the spread of H7N9 influenza in China. *PLoS One* **13**, e0208884 (2018).
19. J. Peiris, L. Poon, Y. Guan, Surveillance of animal influenza for pandemic preparedness. *Science* **335**, 1173–1174 (2012).
20. H. Yu *et al.*, Effect of closure of live poultry markets on poultry-to-person transmission of avian influenza A H7N9 virus: An ecological study. *Lancet* **383**, 541–548 (2014).
21. J. Xu, S. Lu, H. Wang, C. Chen, Reducing exposure to avian influenza H7N9. *Lancet* **381**, 1815–1816 (2013).
22. W. Wang *et al.*, Effectiveness of live poultry market interventions on human infection with avian influenza A (H7N9) virus, China. *Emerging Infect. Dis.* **26**, 891 (2020).
23. Z. Yi *et al.*, Exploring the determinants of influenza A/H7N9 control intervention efficacy in China: Disentangling the effect of the '1110'policy and poultry vaccination. *Transboundary Emerging Dis.* **69**, e1982–e1991 (2022).
24. X. Zeng *et al.*, Vaccination of poultry successfully eliminated human infection with H7N9 virus in China. *Sci. China Life Sci.* **61**, 1465–1473 (2018).
25. X. Zhang, T. Luo, Y. Shen, Deciphering the sharp decrease in H7N9 human infections. *Trends Microbiol.* **26**, 971–973 (2018).
26. Y. He *et al.*, Live poultry market closure and control of avian influenza A (H7N9), Shanghai, China. *Emerging Infect. Dis.* **20**, 1565 (2014).
27. Y. Teng *et al.*, Contact reductions from live poultry market closures limit the epidemic of human infections with H7N9 influenza. *J. Infect.* **76**, 295–304 (2018).
28. J. Chen *et al.*, Emergence of novel avian origin H7N9 viruses after introduction of H7-Re3 and rLN79 vaccine strains to China. *Transboundary Emerging Dis.* **69**, 213–220 (2022).
29. D. He *et al.*, Reintroduction of highly pathogenic avian influenza A H7N9 virus in southwestern China. *Virus Genes.* 10.1007/s11262-023-01974-4 (2023).
30. R. M. Anderson, R. M. May, Population biology of infectious diseases: Part I. *Nature* **280**, 361–367 (1979).
31. Y.-H. Hsieh, J. Wu, J. Fang, Y. Yang, J. Lou, Quantification of bird-to-bird and bird-to-human infections during 2013 novel H7N9 avian influenza outbreak in China. *PLoS One* **9**, e111834 (2014).
32. V. Virlogeux *et al.*, Evaluation of animal-to-human and human-to-human transmission of influenza A (H7N9) virus in China, 2013–15. *Sci. Rep.* **8**, 1–7 (2018).
33. R. Li *et al.*, Inference and forecast of H7N9 Influenza in China, 2013 to 2015. *Eurosurveillance* **22**, 30462 (2017).
34. Y. Xiao, X. Sun, S. Tang, J. Wu, Transmission potential of the novel avian influenza A (H7N9) infection in mainland China. *J. Theor. Biol.* **352**, 1–5 (2014).
35. Z. Liu, C.-T. Fang, A modeling study of human infections with avian influenza A H7N9 virus in mainland China. *Int. J. Infect. Dis.* **41**, 73–78 (2015).
36. A. J. Kucharski, H. L. Mills, C. A. Donnelly, S. Riley, Transmission potential of influenza A (H7N9) virus, China, 2013–2014. *Emerging Infect. Dis.* **21**, 852 (2015).
37. G. Chowell, L. Simonsen, S. Towers, M. A. Miller, C. Viboud, Transmission potential of influenza A/H7N9, February to May 2013, China. *BMC Med.* **11**, 1–13 (2013).

38. H. Nishiura, K. Mizumoto, K. Ejima, How to interpret the transmissibility of novel influenza A (H7N9): An analysis of initial epidemiological data of human cases from China. *Theor. Biol. Med. Model.* **10**, 1–9 (2013).

39. Y. Qin *et al.*, Differences in the epidemiology of human cases of avian influenza A (H7N9) and A (H5N1) viruses infection. *Clin. Infect. Dis.* **61**, 563–571 (2015).

40. Y. Yang *et al.*, Household transmissibility of avian influenza A (H7N9) virus, China, February to May 2013 and October 2013 to March 2014. *Eurosurveillance* **20**, 21056 (2015).

41. G. Zhu *et al.*, Different intervention strategies toward live poultry markets against avian influenza A (H7N9) virus: Model-based assessment. *Environ. Res.* **198**, 110465 (2021).

42. M. J. Pantin-Jackwood *et al.*, Role of poultry in the spread of novel H7N9 influenza virus in China. *J. Virol.* **88**, 5381–5390 (2014).

43. D. Kalthoff *et al.*, Avian influenza H7N9/13 and H7N7/13: A comparative virulence study in chickens, pigeons, and ferrets. *J. Virol.* **88**, 9153–9165 (2014).

44. C. Guinat *et al.*, What can phylodynamics bring to animal health research? *Trends Ecol. Evol.* **36**, 837–847 (2021).

45. B. T. Grenfell *et al.*, Unifying the epidemiological and evolutionary dynamics of pathogens. *Science* **303**, 327–332 (2004).

46. T. Stadler, S. Bonhoeffer, Uncovering epidemiological dynamics in heterogeneous host populations using phylogenetic methods. *Philos. Trans. R. Soc. B. Biol. Sci.* **368**, 20120198 (2013).

47. T. Stadler, D. Kühnert, S. Bonhoeffer, A. J. Drummond, Birth-death skyline plot reveals temporal changes of epidemic spread in HIV and hepatitis C virus (HCV). *Proc. Natl. Acad. Sci. U.S.A.* **110**, 228–233 (2013).

48. T. Stadler *et al.*, Estimating the basic reproductive number from viral sequence data. *Mol. Biol. Evol.* **29**, 347–357 (2012).

49. T. Stadler, D. Kühnert, D. A. Rasmussen, L. du Plessis, Insights into the early epidemic spread of Ebola in Sierra Leone provided by viral sequence data. *PLoS Curr.* **6** (2014), 10.1371/currents. outbreaks.02bc6d927ecee7bbd33532ec8ba6a25f.

50. T. G. Vaughan *et al.*, Estimating epidemic incidence and prevalence from genomic data. *Mol. Biol. Evol.* **36**, 1804–1816 (2019).

51. T. G. Vaughan, D. Kühnert, A. Popinga, D. Welch, A. J. Drummond, Efficient Bayesian inference under the structured coalescent. *Bioinformatics* **30**, 2272–2279 (2014).

52. R. Gao *et al.*, Human infection with a novel avian-origin influenza A (H7N9) virus. *N. Engl. J. Med.* **368**, 1888–1897 (2013).

53. H. Zhu, T.T.-Y. Lam, D. K. Smith, Y. Guan, Emergence and development of H7N9 influenza viruses in China. *Curr. Opin. Virol.* **16**, 106–113 (2016).

54. X. Wang *et al.*, Assessment of human-to-human transmissibility of avian influenza A (H7N9) virus across 5 waves by analyzing clusters of case patients in mainland China, 2013–2017. *Clin. Infect. Dis.* **68**, 623–631 (2019).

55. X. Xiao *et al.*, Transmission of avian influenza A (H7N9) virus from father to child: A report of limited person-to-person transmission, Guangzhou, China, January 2014. *Eurosurveillance* **19**, 20837 (2014).

56. EMPRES-i, Lastest reported events. Avian Influenza A(H7N9) virus, China 2013–2017. Available at: https://EMPRES-i.empres-i.apps.fao.org (Accessed 12 January 2022).

57. C. M. Bui, D. C. Adam, E. Njoto, M. Scotch, C. R. MacIntyre, Characterising routes of H5N1 and H7N9 spread in China using Bayesian phylogeographical analysis. *Emerging Microbes Infect.* **7**, 1–8 (2018).

58. J. Wu *et al.*, Effect of live poultry market interventions on Influenza A(H7N9) Virus, Guangdong, China. *Emerg Infect. Dis.* **22**, 2104–2112 (2016).

59. Q. Yang *et al.*, Assessing the role of live poultry trade in community-structured transmission of avian influenza in China. *Proc. Natl. Acad. Sci. U.S.A.* **117**, 5949–5954 (2020).

60. C. Guinat, Disentangling the role of poultry farms and wild birds in the spread of highly pathogenic avian influenza virus H5N8 in Europe. 2021.10.22.465255. https://www.biorxiv.org/content/10.1101/2021.10.22.465255v1 (2021), 10.1101/2021.10.22.465255.

61. J. Zhang *et al.*, Evolution and antigenic drift of influenza A (H7N9) Viruses, China, 2017–2019. *Emerging Infect. Dis.* **26**, 1906 (2020).

62. M. Gilbert *et al.*, Predicting the risk of avian influenza A H7N9 infection in live-poultry markets across Asia. *Nat. Commun.* **5**, 4116 (2014).

63. C. Li, H. Chen, H7N9 influenza virus in China. *Cold Spring Harb. Perspect. Med.* **11**, a038349 (2021).

64. H. Yu *et al.*, Comparative pathogenicity and transmissibility of the H7N9 highly pathogenic avian influenza virus and the H7N9 low pathogenic avian influenza virus in chickens. *Viruses* **11**, 1047 (2019).

65. M. Kang *et al.*, Epidemiology of human infections with highly pathogenic avian influenza A(H7N9) virus in Guangdong, 2016 to 2017. *Euro Surveill.* **22**, 30568 (2017).

66. N. Xiang *et al.*, Comparison of the first three waves of avian influenza A (H7N9) virus circulation in the mainland of the People's Republic of China. *BMC Infect. Dis.* **16**, 1–12 (2016).

67. N. Xiang *et al.*, Assessing change in avian influenza A (H7N9) virus infections during the fourth epidemic–China, September 2015–August 2016. *MMWR Morb. Mortal. Wkly. Rep.* **65**, 1390–1394 (2016).

68. D. Wu *et al.*, Poultry farms as a source of avian influenza A (H7N9) virus reassortment and human infection. *Sci. Rep.* **5**, 7630 (2015).

69. B. Shi, S. Xia, G.-J. Yang, X.-N. Zhou, J. Liu, Inferring the potential risks of H7N9 infection by spatiotemporally characterizing bird migration and poultry distribution in eastern China. *Infect. Dis. Poverty* **2**, 1–10 (2013).

70. Y. Xing, L. Song, G.-Q. Sun, Z. Jin, J. Zhang, Assessing reappearance factors of H7N9 avian influenza in China. *Appl. Mathemat. Comput.* **309**, 192–204 (2017).

71. J. C. Jones *et al.*, Possible role of songbirds and parakeets in transmission of influenza A (H7N9) virus to humans. *Emerging Infect. Dis.* **20**, 380 (2014).

72. B. Zhao *et al.*, Novel avian influenza A (H7N9) virus in tree sparrow, Shanghai, China, 2013. *Emerging Infect. Dis.* **20**, 850 (2014).

73. Q. Lin, Z. Lin, A. P. Chiu, D. He, Seasonality of influenza A (H7N9) virus in China–fitting simple epidemic models to human cases. *PLoS One* **11**, e0151333 (2016).

74. R. J. Soares Magalhães *et al.*, Live poultry trade in Southern China provinces and HPAIV H5N1 infection in humans and poultry: The role of Chinese New Year festivities. *PLoS One* **7**, e49712 (2012).

75. M. Fan *et al.*, Human influenza A(H7N9) virus infection associated with poultry farm, Northeastern China. *Emerg Infect. Dis.* **20**, 1902–1905 (2014).

76. K. M. Pepin *et al.*, Minimizing the threat of pandemic emergence from avian influenza in poultry systems. *BMC Infect. Dis.* **13**, 1–6 (2013).

77. K. Katoh, D. M. Standley, MAFFT multiple sequence alignment software version 7: Improvements in performance and usability. *Mol. Biol. Evol.* **30**, 772–780 (2013).

78. A. Larsson, AliView: A fast and lightweight alignment viewer and editor for large datasets. *Bioinformatics* **30**, 3276–3278 (2014).

79. L. Yang *et al.*, Genesis and spread of newly emerged highly pathogenic H7N9 avian viruses in mainland China. *J. Virol.* **91**, e01277-17 (2017).

80. D. L. Ayres *et al.*, BEAGLE: An application programming interface and high-performance computing library for statistical phylogenetics. *Syst. Biol.* **61**, 170–173 (2012).

81. J. Scire, J. Barido-Sottani, D. Kühnert, T. G. Vaughan, T. Stadler, Improved multi-type birth-death phylodynamic inference in BEAST 2. *Viruses* **14**, 1648 (2022).

82. D. Kühnert, T. Stadler, T. G. Vaughan, A. J. Drummond, Phylodynamics with migration: A computational framework to quantify population structure from genomic data. *Mol. Biol. Evol.* **33**, 2102–2116 (2016).

83. X. Zhou *et al.*, Geographical variation in the risk of H7N9 human infections in China: Implications for risk-based surveillance. *Sci. Rep.* **10**, 1–10 (2020).

84. Q. Li *et al.*, Epidemiology of human infections with avian influenza A (H7N9) virus in China. *N. Engl. J. Med.* **370**, 520–532 (2014).

85. L. Zhou *et al.*, Risk factors for influenza A (H7N9) disease in China, A matched case control study, october 2014 to april 2015. *Open Forum Infect. Dis.* **3**, ofw182 (2016).

86. B. Shapiro, A. Rambaut, A. J. Drummond, Choosing appropriate substitution models for the phylogenetic analysis of protein-coding sequences. *Mol. Biol. Evol.* **23**, 7–9 (2006).

87. R. Li *et al.*, Live poultry trading drives China's H7N9 viral evolution and geographical network propagation. *Front. Public Health* **6**, 210 (2018).

88. A. J. Drummond, S. Y. W. Ho, M. J. Phillips, A. Rambaut, Relaxed phylogenetics and dating with confidence. *PLoS Biol.* **4**, e88 (2006).

89. L. Lu, A. J. L. Brown, S. J. Lycett, Quantifying predictors for the spatial diffusion of avian influenza virus in China. *BMC Evol. Biol.* **17**, 1–14 (2017).

90. J. Lu *et al.*, Molecular evolution, diversity, and adaptation of influenza A (H7N9) viruses in China. *Emerging Infect. Dis.* **24**, 1795 (2018).

91. L. Zhou *et al.*, Preliminary epidemiology of human infections with highly pathogenic Avian influenza A(H7N9) virus, China, 2017. *Emerg Infect. Dis.* **23**, 1355–1359 (2017).

92. R. Bouckaert *et al.*, BEAST 2: A software platform for Bayesian evolutionary analysis. *PLoS Comput. Biol.* **10**, e1003537 (2014).

93. A. Rambaut, A. J. Drummond, D. Xie, G. Baele, M. A. Suchard, Posterior summarization in Bayesian phylogenetics using Tracer 1.7. *Syst. Biol.* **67**, 901 (2018).

94. W. A. Freyman, S. Höhna, Stochastic character mapping of state-dependent diversification reveals the tempo of evolutionary decline in self-compatible Onagraceae lineages. *Syst. Biol.* **68**, 505–519 (2019).

95. G. Yu, D. K. Smith, H. Zhu, Y. Guan, T. T. Lam, ggtree: An R package for visualization and annotation of phylogenetic trees with their covariates and other associated data. *Methods Ecol. Evol.* **8**, 28–36 (2017).

96. R Core Team, R: A language and environment for statistical computing (Version 4.2.2, R Foundation for Statistical Computing, Vienna, Austria, 2022).

97. GISAID, H7N9 sequences and associated metadata. *GISAID Platform.* http://www.gisaid.org. Accessed 12 January 2022.

98. FAO, Overview of H7N9 outbreaks. *EMPRES-i.* https://empres-i.apps.fao.org. Accessed 12 January 2022.

99. C. Guinat, H7N9_bdmm-prime. *GitHub.* https://github.com/ClaireGuinat/h7n9_bdmm-prime. Accessed 12 January 2022.